

LETTER TO THE EDITOR

Resolving the circumbinary dust disk surrounding HH 30^{*}

S. Guilloteau^{1,2}, A. Dutrey^{1,2}, J. Pety^{3,4}, and F. Gueth³

¹ Université Bordeaux 1; Laboratoire d'Astrophysique de Bordeaux (LAB), France
e-mail: [Stephane.Guilloteau;Anne.Dutrey]@obs.u-bordeaux1.fr

² CNRS/INSU – UMR5804, BP 89, 33270 Floirac, France

³ IRAM, 300 rue de la Piscine, 38400 Saint Martin d'Hères, France
e-mail: [pety;gueth]@iram.fr

⁴ LERMA, UMR 8112, CNRS, Observatoire de Paris, 61 Av. de l'Observatoire, 75014 Paris, France

Received 12 November 2007 / Accepted 5 December 2007

ABSTRACT

Context. The jet-disk connection is an important part of the star formation process. HH 30 is a rare and beautiful example of a system exhibiting a flared edge-on disk, an optical jet and a CO molecular outflow. A recent analysis of the jet wiggling has revealed that the central star is in reality a binary object. Therefore, the dust and gas disk observed around HH 30 is circumbinary.

Aims. In this paper, we attempt to better constrain the system (disk + stars) properties, as well as the system age.

Methods. We obtained very high angular resolution ($\sim 0.4''$) observations in continuum at 1.3 mm with the IRAM interferometer. A standard disk model is used to fit the continuum and line data in the Fourier-plane and derive the disk properties.

Results. We find that the disk of HH 30 is truncated at an inner radius 37 ± 4 AU. The simplest explanation is tidal truncation in a binary system. This confirms the binarity of the HH 30 system, which consists of two stars on a low eccentricity, 15 AU semi-major axis orbit. The jet wiggling is due to orbital motion. The mass ratio is poorly constrained. The system age may be less than 2 Myr. The disk is optically thin at 1.3 mm and the dust opacity index, $\beta \approx 0.4$, indicates the presence of cm size grains.

Conclusions. These observations confirm that HH 30, often presented as an archetypal example of the jet-disk paradigm, is a binary star, with one of the components at the origin of the optical jet. This suggests that many other objects similar to HH 30 may be unknown binary or multiple systems. These new data confirm that high angular resolution observations at millimeter wavelengths are powerful tools to unveil the inner dust disk properties. In this domain, ALMA will likely change our observational vision of these objects.

Key words. stars: formation – stars: circumstellar matter – ISM: molecules – stars: individual: HH30

1. Introduction

HST observations of the HH 30 young stellar system, located in the Taurus-Auriga cloud at 140 pc, revealed a flared, almost edge-on, dust disk seen in scattered light, driving a linear perpendicular jet (Burrows et al. 1996). This source has since been extensively studied. In a previous paper (Pety et al. 2006, hereafter Paper I), we investigated the dust and gas disk surrounding HH 30 at an angular resolution of $\sim 1''$ or 140 AU, at the Taurus distance. We studied the properties of the dust and CO disk but also characterized the CO outflow as close as possible to the disk surface. Optical observations of the jet over more than ten years are now available and Anglada et al. (2007) recently measured the jet proper motions. Surprisingly, their detailed analysis revealed that the central object is likely a binary star. Modeling the jet proper motions, they found two possible solutions for the binary orbit: either the jet is wiggling due to precession and therefore the jet source has a mass $\sim 0.1-1 M_{\odot}$, the companion being sub-stellar (mass $< 0.01 M_{\odot}$) with an orbital period < 1 yr; or the jet wiggling is due to orbital motion, the binary having an orbital period of ~ 53 yr and a total mass within the range $0.25-2 M_{\odot}$.

In winter 2007, we used the new A configuration of the IRAM array to map HH 30 in continuum at 1.3 mm and in CO $J = 2-1$ line. Our new observations have an angular resolution of $\sim 0.3''$ (or ~ 50 AU at the Taurus distance) in the direction parallel to the disk, a gain of 3 compared to Paper I. We present here the new data a combination of the new and the old data and we focus on the continuum data analysis of the disk and on the binary properties. In a third paper (Pety et al. 2008, in prep.), we will present a detailed study of the CO jet.

2. Observation and data reduction

We only discuss here the new data and the proper motion correction. The two previous data sets at 90 and 220 GHz are described in Paper I.

The observations were carried out on 2007, Feb. 3rd, with the 6 antennas of the IRAM Plateau de Bure interferometer in the largest configuration (longest baseline about 760 m or 590 $k\lambda$). We observed HH30 near 230 GHz, in dual polarization, with the correlator providing a total effective bandwidth of about 1.8 GHz. The source was observed for ~ 9 h, leaving a *total on-source* observing time of 6 h. The rms phase noise was between 19 and 53° at 1.3 mm. The seeing, estimated from observations of the calibrators, was better than $\sim 0.15''$ after calibration.

* PdBI is operated by IRAM, which is supported by INSU/CNRS (France), MPG (Germany), and IGN (Spain).

All data were reduced using the GILDAS¹ software supported at IRAM (Pety 2005). Standard calibration methods using nearby calibrators were applied to all the PdBI data.

To recombine all observations, the flux scales were carefully checked, by comparing the visibilities on short baselines (following the procedure described in Paper I). This was performed independently on two sources: HH 30 and MWC 480 (used as secondary calibrator, as in Piétu et al. 2007). We found a consistent flux scale to better than 10% accuracy. The 230 GHz and 220 GHz data were combined after correction, assuming an apparent spectral index α of the emission of 2.3 (in agreement with Paper I); this is only a 10% correction.

Separate imaging of the three data sets revealed a slight shift in positions between the earlier data (1997) and the most recent ones (2007), of $0.00 \pm 0.04''$ in RA and $-0.15 \pm 0.03''$ in Dec. The magnitude and direction of the shift are consistent with the expected proper motion in this region of Taurus in ten years. The average proper motion of the young stars in Taurus is $(4, -22) \mu\text{as/yr}$ (based on HL Tau, XZ Tau, LkHa 358, MWC 480, AB Aur, SU Aur, BP Tau and DM Tau, see Ducourant et al. 2005). Taking only the stars nearest to HH 30 (HL Tau, XZ Tau and LkHa 358), the average motion is $(9, -19) \mu\text{as/yr}$, while the two most accurate measurements indicate $(1, -24) \mu\text{as/yr}$ (MWC 480 and AB Aur). Considering the uncertainties, we recombined our measurements by assuming a proper motion value of $(0, -20) \mu\text{as/yr}$ for HH 30.

A natural weighting was applied to produce the final image presented in Fig. 1. It gives a resolution of $0.59 \times 0.32''$ at PA = 22° , and an rms noise level of 0.185 mJy/beam, or 23 mK in brightness. The peak brightness in the image is 0.43 K. The linear resolution along the HH 30 disk mid-plane is 45 AU, while it is 83 AU in the perpendicular direction.

3. Results and analysis

The dust image at 1.3 mm is clearly not centrally peaked but reveals two bright peaks located at $0.3''$ or 50 AU from the emission centroid.

The UV data can be adequately fitted by two uniform brightness, elliptical disks. However, a major argument against this possibility comes from the ^{13}CO , which shows a simple Keplerian rotation exactly around the mid-point between the two dust emission peaks, while in the case of two disks, it would either peak on one of the two, or show a more complex pattern due to the superposition of the two disks. We thus conclude that we are seeing a single disk with a minimum of brightness towards the center of mass of the system.

The low apparent surface brightness most likely rules out significant optical thickness. To explain a brightness of only 0.5 K, with a typical dust temperature of about 10 K, by an optically thick layer would imply a dilution factor larger than 20. As the disk is radially well resolved, this would require i) that the layer is geometrically thin, of typical thickness 20 times smaller than the resolution across the disk thickness, or only 3–4 AU, and ii) that the layer is seen edge-on – the inclination must not differ from 90° by more than the thickness to radius ratio, i.e. about 2° . Such a high inclination is not supported by the data (see Paper I and detailed modeling below).

Accordingly, the two peaks likely correspond to maxima of column densities. The dust distribution is thus reminiscent of

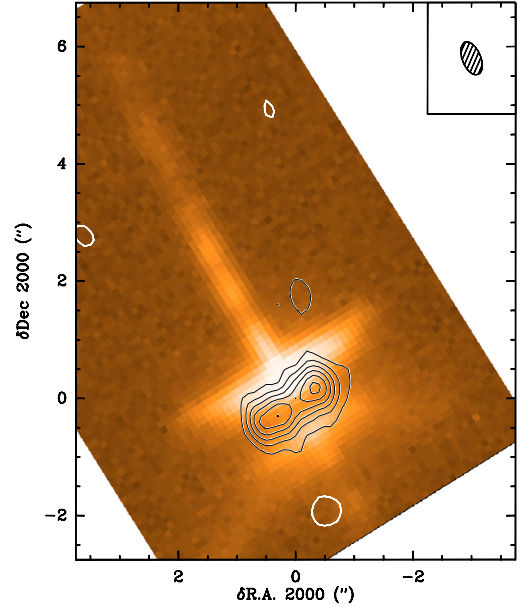


Fig. 1. Superimposition of the PdBI 1.30 mm continuum map on the HST data. The spatial resolution is $0.59 \times 0.32''$ at PA 22° . The center of projection is RA = $04^{\text{h}}31^{\text{m}}37.469$ and Dec = $18^\circ12'24''.22$ in J2000. Contour levels start at and are spaced by $3\sigma = 0.56$ mJy/beam, corresponding to 68 mK. The registration of the HST image is approximate, as the positions given by Anglada et al. (2007) and Cotera et al. (2001) differ by $1''$.

Table 1. Parameters of the dust disk around HH 30 derived from the model fits of the continuum emission. q and p have been fixed (see Sect. 3). The error bars are the 1σ formal errors from the fit. For the scale-height, $h(r) = h_{100} \times (r/100 \text{ AU})^h$ using notations of Paper I, we assume hydrostatic equilibrium, so $h = 1.5$ for $q = 0$, and h_{100} is derived from T_{100} .

Parameters	Values	Parameters	Values
PA ($^\circ$)	35 ± 1	Σ_{100} (cm^{-2})	$2.2 \pm 0.2 \times 10^{23}$
i ($^\circ$)	81 ± 2	p	0, fixed
R_{in}^c (AU)	40 ± 5	h_{100} (AU)	11 ± 3
R_{out}^c (AU)	128 ± 3	h	1.5, fixed
T_{100} (K)	9 ± 3	β	0.4 ± 0.1
q	0, fixed		

that of Lk Ca 15 (Piétu et al. 2006), with a significant drop in column density in the inner 50 AU.

We have modeled the disk emission using the same method as Piétu et al. (2006), with simultaneous fitting of the new combined 1.3 mm data and of the 3.4 mm data from Paper I by a truncated disk with power laws for the surface density and temperature profile. We used a stellar mass of $0.45 M_\odot$, as derived from Paper I. The parameters of the best fit model are given in Table 1. In our derivation, we assumed the exponent of the surface density $p = 0$, and the exponent of the temperature law $q = 0$, and we assumed hydrostatic equilibrium. The analysis confirms that HH 30 has an inner cavity of 40 ± 5 AU radius, very much like Lk Ca 15.

As in LkCa15 (Piétu et al. 2006), there is some degeneracy between R_{in} and $p + q$. The data can be fitted with a small hole radius for $p + q = -1.5$ (which, for $q \geq 0$, implies a density rising with radius), while any positive value for $p + q$ would result in larger sizes, i.e., a larger inner radius (and hole) and a larger

¹ See <http://www.iram.fr/IRAMFR/GILDAS> for more information about the GILDAS softwares.

outer disk radius. $p + q \geq 1.5$ is excluded at the 3σ level. We thus take the best fit value given for $p + q = 0$, by assuming p and q equal zero, as the most physical solution.

Since the new continuum data indicate the presence of an inner cavity, we have re-analyzed the ^{13}CO data from Paper I to search for the presence of an inner hole in the CO distribution. The best formal ^{13}CO fit indicates an inner radius of 33 ± 7 AU. This radius is essentially constrained by the lack of emission at velocities larger than 3 km s^{-1} , and thus independent of any choice of p or q .

Combining the dust and ^{13}CO results gives a weighted mean radius $R_{\text{in}} = 37 \pm 4$ AU. A disk with an inner cavity of ~ 40 AU radius thus provides a consistent explanation of our observations.

4. Discussion

4.1. The dust disk properties

The best disk model provides four interesting values: 1) the inclination, 2) the temperature and scale height, 3) the dust emissivity spectral index β , and 4) the outer radius, all of which are given in Table 1.

- *Inclination*: we find the inclination to be $81 \pm 2^\circ$. This is in excellent agreement with the ^{13}CO data from Paper I, $81 \pm 3^\circ$. It confirms that the disk is not exactly edge-on, and rules out the possibility of a significant contribution from a geometrically thin but optically thick dust layer.
- *Scale height and temperature*: the apparent scale height obtained from the continuum is 11 ± 3 AU at 100 AU (assuming hydrostatic equilibrium with $q = 0$, and thus a flaring exponent $h = 1.5$), corresponding to the hydrostatic scale height for a temperature of 9–10 K only. This is in agreement with the kinetic temperature of ≈ 12 K found from ^{13}CO in Paper I. It is much smaller than the value of 34 K found by Burrows et al. (1996), from scattered light images that sample the small particles high above the disk. It confirms the vertical temperature gradient, which was found from ^{13}CO in Paper I.
- *Spectral index*: with a value $\beta = 0.4 \pm 0.1$, the spectral index of the dust emissivity is rather flat. This is in general attributed to the presence of large grains. Very few disks display such a low value, the average being rather around 1.0. Draine (2006) has shown that, under the assumption of power law $dn/da \propto a^{-d}$ for the size distribution of grains, and provided $a_{\text{max}} > 3\lambda$, the mm spectral index is well represented by $\beta = (d - 3)\beta_s$, where β_s is the small grain spectral index. Since $\beta_s \approx 1.8$ for interstellar grains, our measurement would imply $d \approx 3.2$ (see Draine 2006, Fig. 6). Note that our mass is scaled according to the Beckwith et al. (1990) prescription, $\kappa(\nu) = 0.1(\nu/10^{12} \text{ Hz})^\beta$, i.e. $\kappa(1.3 \text{ mm}) = 0.055 \text{ cm}^2 \text{ g}^{-1}$ (of dust+gas).
- *Outer radius*: the best fit provides an outer radius of ≈ 130 AU. This can be made somewhat larger, but not very significantly (< 150 AU), by setting $p > 0$. In any case, it is much smaller than the outer radius derived from either the ^{13}CO in Paper I or the optical images (Burrows et al. 1996), which are in the range of 250–400 AU. It indicates a significant drop of the mm dust opacity beyond $R > 130$ AU. This may be due to a change in H_2 surface density at this radius, or to the fact that the large particles have already migrated closer to the central stars.

4.2. The inner cavity: tidal clearing by a binary

Anglada et al. (2007) suggested two possibilities to explain the jet wiggling of HH 30: (i) orbital motion of the jet source, or (ii) precession of the jet direction induced by a companion. In the second case, the jet would come from the primary, and the orbital separation would be very small, of the order 0.3 AU. The independent discovery of an inner cavity strengthens this statement, since the easiest explanation for a cavity is tidal disturbance by a companion, as exemplified by the GG Tau system (Dutrey et al. 1994; Guilloteau et al. 1999).

For a tidally cleared cavity in a binary system, the inner radius is determined to first order by the first orbital resonance that lies in near circular equipotential (Artymowicz & Lubow 1994; Dutrey et al. 1994). This radius depends on the orbital semi-major axis a , the mass ratio μ and the eccentricity e of the binary.

The eccentricity e can only be constrained from the level of asymmetries in the jet wiggling since the shape of the oscillations is determined by the eccentricity and the angle between the orbital major axis and the line of sight (see for example González & Raga 2004). We have verified that the very symmetrical aspect of the jet wiggling indicates eccentricities smaller than $e = 0.1$. The orbit is thus nearly circular.

Constraints on a and μ can be derived both from Anglada et al. (2007) and our new results. Let M_j be the mass of the star from which the jet is launched, and M_o the mass of the other star (M_* being the total stellar mass). We define μ from $M_j = (1 - \mu) M_*$ and $M_o = \mu M_*$. In case (i) of Anglada et al. (2007), under the assumption of a circular orbit, the jet source orbital radius $R_{\text{jet}} = 8.9 \pm 0.9$ AU, and the period $P_{\text{jet}} = 53 \pm 15$ yr, are linked to the stellar masses by

$$M_* = R_{\text{jet}}^3 P_{\text{jet}}^{-2} \mu^{-3} \quad \text{and} \quad \mu = R_{\text{jet}} (P_{\text{jet}}^2 M_*)^{-1/3}. \quad (1)$$

The binary semi-major axis of the orbit is

$$a_{\text{jet}} = R_{\text{jet}} / \mu = (P_{\text{jet}}^2 M_*)^{1/3}. \quad (2)$$

Using $M_* = 0.45 \pm 0.04 M_\odot$ from Paper I, we derive $a_{\text{jet}} = 10.8 \pm 2.3$ AU and $\mu = 0.82 \pm 0.27$.

To constrain a and μ from the cavity size, we follow Dutrey et al. (1994). The effective potential of a test particle in the rotating frame of the stars is given by

$$\Phi(r, t) = -\frac{M_j G}{|r_j - r|} - \frac{M_o G}{|r_o - r|} - \frac{1}{2} \Omega_{\text{CM}}^2 r^2 \quad (3)$$

r being the distance of the particle from the center of mass (CM), Ω_{CM} the instantaneous angular velocity of the two stars around (CM), M_j and M_o the masses of the stars located at distances r_j and r_o from (CM). This expression does not include the Coriolis effect. Figure 2 summarizes a possible configuration for $e = 0.1$, $M_j = 0.15$, $M_o = 0.30 M_\odot$ and $a = 15$ AU, when the stars are at the apastron. The first stable orbits appear beyond the 3:1 resonance. This result is valid for all but the most extreme mass ratios ($\mu > 0.9$ or $\mu < 0.1$), for which orbits near the 2:1 resonance can become stable for $e < 0.1$. Similar results have been obtained through the study of invariant loops by Pichardo et al. (2005). As the 3:1 resonance is at $2.08a$, our inner radius $R_{\text{in}} = 37 \pm 4$ AU can be caused by a binary system with $a_{\text{cavity}} = 18 \pm 2$ AU.

This is somewhat larger than a_{jet} derived from the jet wiggling, but within an acceptable margin given the roughness of the approximations used in deriving the constraints on the orbits. Increasing the eccentricity e to 0.2 would offer a better agreement, as the inner radius reaches the 4:1 resonance at $2.52a$, but

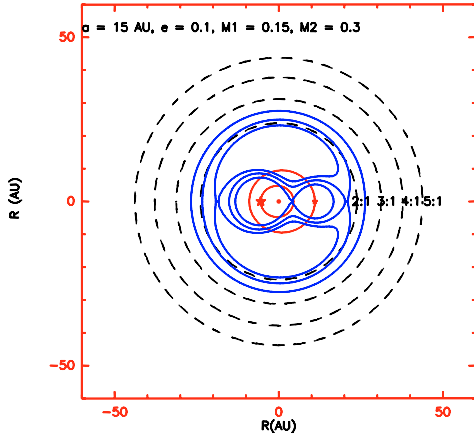


Fig. 2. Roche equipotentials for a binary system of stellar masses 0.15 and $0.3 M_{\odot}$ (solid blue lines). The dot gives the location of the mass center. The thick (red) ellipses are the stellar orbit around the center of mass. The dashed lines correspond to equipotentials of the orbital resonances 2:1, 3:1, 4:1 and 5:1. The stars have been put at the apastron.

seems difficult to reconcile with the very symmetric wiggling pattern.

In any case, the above result clearly shows that tidal effects induced in the case (ii) (jet precession due to two stars separated by 0.3 AU) cannot at all explain the large inner hole that we observe in the mm continuum.

Combining all constraints, we thus conclude that HH 30 is a binary of separation around 15 AU, period 80 yr and total mass $0.5 M_{\odot}$, but the mass ratio remains poorly constrained. In such a system, the *circumstellar* disks will be truncated with an outer radius smaller than $\sim a/3$, i.e., 5 AU. This implies that the optical jet comes from an even smaller region. The binarity of HH 30 changes its age determination from its location on theoretical

evolutionary tracks: splitting the luminosity into two stars of lower masses implies younger objects. The total luminosity and spectral types of HH 30 are poorly known (see Paper I for a discussion). Assuming that both stars have nearly equal masses, their positions in a (T_{eff}, L) diagram are consistent with a spectral type around M3 ($T_{\text{eff}} \approx 3500$ K) and age 1–2 Myr using the tracks from Siess et al. (2000) or Palla & Stahler (1999). The tracks from Baraffe et al. (1998) gives somewhat younger ages (see Fig. 6 of Simon et al. 2000). A younger age may be in better agreement with the existence of the powerful collimated jet and the CO outflow.

Acknowledgements. We acknowledge the IRAM staff at Plateau de Bure and Grenoble for carrying out the observations.

References

- Anglada, G., López, R., Estalella, R., et al. 2007, *AJ*, 133, 2799
 Artymowicz, P., & Lubow, S. H. 1994, *ApJ*, 421, 651
 Baraffe, I., Chabrier, G., Allard, F., & Hauschildt, P. H. 1998, *A&A*, 337, 403
 Beckwith, S. V. W., Sargent, A. I., Chini, R. S., & Guesten, R. 1990, *AJ*, 99, 924
 Burrows, C. J., Stapelfeldt, K. R., Watson, A. M., et al. 1996, *ApJ*, 473, 437
 Cotera, A. S., Whitney, B. A., Young, E., et al. 2001, *ApJ*, 556, 958
 Draine, B. T. 2006, *ApJ*, 636, 1114
 Ducourant, C., Teixeira, R., Périé, J. P., et al. 2005, *A&A*, 438, 769
 Dutrey, A., Guilloteau, S., & Simon, M. 1994, *A&A*, 286, 149
 González, R. F., & Raga, A. C. 2004, *Rev. Mex. Astron. Astrofis.*, 40, 61
 Guilloteau, S., Dutrey, A., & Simon, M. 1999, *A&A*, 348, 570
 Palla, F., & Stahler, S. W. 1999, *ApJ*, 525, 772
 Pety, J. 2005, in *SF2A-2005: Semaine de l'Astrophysique Française*, ed. F. Casoli, T. Contini, J. M. Hameury, & L. Pagani, 721
 Pety, J., Gueth, F., Guilloteau, S., & Dutrey, A. 2006, *A&A*, 458, 841
 Pichardo, B., Sparke, L. S., & Aguilar, L. A. 2005, *MNRAS*, 359, 521
 Piétu, V., Dutrey, A., Guilloteau, S., Chapillon, E., & Pety, J. 2006, *A&A*, 460, L43
 Piétu, V., Dutrey, A., & Guilloteau, S. 2007, *A&A*, 467, 163
 Siess, L., Dufour, E., & Forestini, M. 2000, *A&A*, 358, 593
 Simon, M., Dutrey, A., & Guilloteau, S. 2000, *ApJ*, 545, 1034